American Mineralogist, Volume 79, pages 168–174, 1994

Hollandite-type phases: Geometric consideration of unit-cell size and symmetry

JINMIN ZHANG, CHARLES W. BURNHAM
Department of Earth and Planetary Sciences, Harvard University, Cambridge, Massachusetts 02138, U.S.A.

ABSTRACT

Equations are derived for predicting the lengths of unit-cell edges and the symmetry of hollandite-type compounds with the general formula $A_{0-2}B_8(O,OH)_{16}$. The unit-cell size of a hollandite-type compound is determined largely by the average B-O bond distance, and additionally by the charge of the B cation (Z_B), the excess size of the tunnel cation (A) relative to the BO_6 octahedral framework (δ_A), and the excess size of the B cation relative to the octahedral cavity (δ_B). These factors are incorporated in the following equations, which accurately estimate the unit-cell edge lengths:

$$a(\text{Å}) = 5.130(r_O + r_B) - 0.0291Z_B + 0.441\delta_A$$

$$c(\text{Å}) = \sqrt{2}(r_O + r_B) + 0.0366Z_B + 0.552\delta_B.$$

The symmetry of a hollandite-type compound is related to the size of the tunnel cation (A). If $r_A > \sqrt{2}(r_O + r_B) - r_O$, the compound cannot be monoclinic, whereas if $r_A < \sqrt{2}(r_O + r_B) - r_O - 0.15$ it cannot be tetragonal. These relationships make it possible to predict the symmetry and unit-cell size of a hollandite-type compound based on composition alone.

INTRODUCTION

Hollandite-type compounds are important to mineralogists and materials scientists. Several types occur as minerals (e.g., hollandite, cryptomelane, priderite, and α-MnO_2), whereas many others have been synthesized. Some hollandite types have special properties such as ferromagnetism (Endo et al., 1976) or superionic conductivity (Beyeler, 1976). The natural phases are important deep-sea minerals (Burns and Burns, 1977). A synthetic rock (SYNROC) containing hollandite as a major constituent has been proposed for use in the storage of radioactive wastes (Ringwood et al., 1979). The common crustal mineral feldspar transforms to the hollandite structure at high pressures and temperatures and may be a repository for light elements and H_2O in the mantle (Zhang et al., 1993). The aluminosilicate hollandite-type compounds are among the few phases so far discovered having both Al and Si in octahedral coordination.

The ideal hollandite structure is tetragonal with the space group $I4/m$ (Fig. 1). The general formula is $A_{0-2}B_8(O,OH)_{16}$, where A is an alkali or alkaline-earth cation and B is usually a mixture of tetravalent and trivalent cations. BO_6 octahedra share edges to form a wall of double chains, each of which shares corners with neighboring walls to form a framework with tunnels that accommodate large A cations and H_2O molecules. The coordination number of A is 8, and the average coordination number of O^{2-} is 4 if the A (tunnel) sites are fully occupied. Atomic coordinates of ideal hollandite are derived in Appendix 1.

It has been recognized that the unit-cell size of a hollandite phase is largely determined by the size of the BO_6 octahedron (Ringwood et al., 1967). One might, however, expect that the size of the tunnel cation and other structural factors would play roles as well, although at present no methods for estimating hollandite unit-cell sizes incorporate such structural factors. Many hollandite phases are tetragonal, but some are monoclinic; which structural factors are most important in determining the symmetry of a particular hollandite phase has been unclear. Although empirical criteria have been suggested, it would be useful to develop criteria that are more clearly associated with specific structural factors and have a better theoretical basis. In this study we have modeled the unit-cell parameters and the symmetry of the hollandite structure based on detailed geometric considerations.

DERIVATIONS

We use effective ionic radii, r_i, taken from Shannon and Prewitt (1969). Basic geometric parameters of a regular BO_6 octahedron include the apex to apex length, $2(r_O + r_B)$, and the O-O edge length, $\sqrt{2}(r_O + r_B)$. The height (parallel to **c**) of the tetragonal coordination prism around the tunnel cation is equal to the octahedral edge length (see Fig. 1). The tunnel edge length, IO2 in Figure 1, is twice the horizontal projection of octahedral edge JO1, or $2\sqrt{2}(r_O + r_B)\cos 30° = \sqrt{6}(r_O + r_B)$. The tunnel edge is also the (001) face diagonal of the tetragonal coordination prism around the tunnel cation. The body diagonal of the tetragonal coordination prism ($=2 \times |\mathbf{AO1}|$)

is thus

$$\sqrt{[\sqrt{6}(r_O + r_B)]^2 + [\sqrt{2}(r_O + r_B)]^2} = 2\sqrt{2}(r_O + r_B).$$

The radius of a tunnel cation that fits perfectly into the tetragonal prism, r_C, must therefore meet the condition $2(r_O + r_C) = 2\sqrt{2}(r_O + r_B)$ from which

$$r_C = \sqrt{2}(r_O + r_B) - r_O. \quad (1)$$

Whereas the length of c corresponds simply to the edge of the BO_6 octahedron, the length of a is not as readily understood. From Figure 1, AA′ is half the (001) unit-cell face diagonal, and the following relationship is observed:

$$AA'^2 = AF^2 + FA'^2. \quad (2)$$

Here AF is the sum of the tunnel edge and the octahedral wall thickness. The wall thickness, HO1, is equal to the apex to base distance of the tetrahedral interstice in the double octahedral chain. As the edge length of the tetrahedral interstice is $\sqrt{2}(r_O + r_B)$, its height is $\sqrt{6}/3[\sqrt{2}(r_O + r_B)] = (2\sqrt{3}/3)(r_O + r_B)$, and

$$AF = \sqrt{6}(r_O + r_B) + \frac{2\sqrt{3}}{3}(r_O + r_B). \quad (3)$$

The following relationships also obtain:

$$A'F = A'G - FG = A'G - HI$$
$$= A'G - \sqrt{(IO1)^2 - (HO1)^2}$$

where A′G is half the tunnel edge, IO1 is an edge of the octahedron, and HO1 is the wall thickness. Thus,

$$A'F = \frac{\sqrt{6}}{2}(r_O + r_B) - \sqrt{[\sqrt{2}(r_O + r_B)]^2 - \left[\frac{2\sqrt{3}}{3}(r_O + r_B)\right]^2}$$
$$= \frac{\sqrt{6}}{6}(r_O + r_B). \quad (4)$$

Substituting relations for A′F and AF into Equation 2, we obtain $AA'^2 = [(\sqrt{6}/6)(r_O + r_B)]^2 + [\sqrt{6}(r_O + r_B) + (2\sqrt{3}/3)(r_O + r_B)]^2$ and

$$AA' = 3.627(r_O + r_B). \quad (5)$$

Then the a axis is

$$a = 2(AA' \cos 45°) = 5.130(r_O + r_B) \quad (6)$$

and the c axis is

$$c = \sqrt{2}(r_O + r_B). \quad (7)$$

Values of a and c calculated using Equations 6 and 7 are systematically larger and smaller, respectively, than observed values. The calculated c/a ratio is $\sqrt{2}/5.130 = 0.276$, but hollandite typically has c/a ratios around 0.3. The larger ratio arises because the BO_6 octahedra are elongated parallel to **c** and shortened perpendicular to **c**

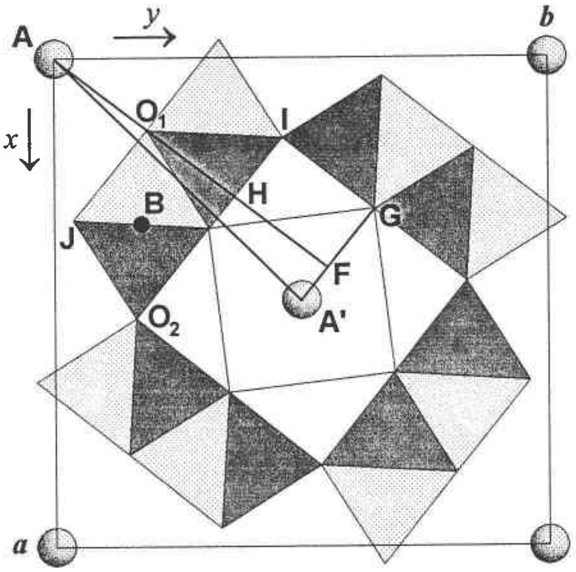

Fig. 1. Schematic c-axis projection of ideal $I4/m$ hollandite structure with regular octahedra. Shaded circles, A and A', represent tunnel cations; solid circle, B, is an octahedral cation. Atoms O1, O2, and B have ideal x and y coordinates derived in the text. The tetragonal prismatic coordination polyhedron surrounding tunnel cation A' is outlined inside the tunnel.

as a consequence of strong cation to cation repulsions across the shared edges in the BO_6 chains.

To account for B-B repulsions, we add a dependence on the valence of B to Equation 7: $c = \sqrt{2}(r_O + r_B) + vZ_B$ where v is the coefficient of proportionality and Z_B is the valence of the B cation. Using observed data for α-MnO_2 (Donnay and Ondik, 1973), we obtain $2.846 = \sqrt{2}(1.38 + 0.54) + 4v$ from which $v \approx 0.0328$ and the equation for calculating c becomes

$$c = \sqrt{2}(r_O + r_B) + 0.0328 Z_B. \quad (8)$$

Equation 8 produces reasonably good estimates of c, especially when c is small. As c increases above 2.9 Å (corresponding to $r_B \sim 0.6$ Å for $Z_B = 4$), however, the deviation from experimental values also increases (see Fig. 2). On the basis of overly simplistic but familiar classical packing considerations, we find that a B cation fits perfectly into the octahedral interstice when $r_B = 0.414 r_O$; if we use $r_O = 1.38$ Å ($^{[3]}O^{2-}$: Shannon and Prewitt, 1969), the critical cation radius is 0.57 Å, close to the value of r_B (0.6 Å) at which the experimental data begin to deviate from Equation 8. This suggests that octahedral distortions increase, causing further elongation of c, when the classical octahedral critical radius ratio is exceeded. We include the anticipated effect of this distortion by introducing an additional dependence of c on δ_B, the amount by which r_B exceeds the critical octahedral cation radius.

The tunnel cation size may also influence the unit-cell dimensions. From the examples of $K_2(MgTi_7)O_{16}$ ($a = 10.157$, $c = 2.974$ Å) and $Rb_2(MgTi_7)O_{16}$ ($a = 10.195$, c

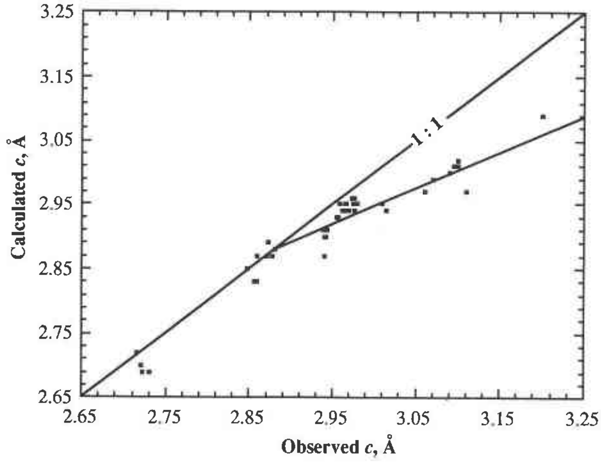

Fig. 2. Calculated c values using Eq. 8, showing deviation from a 1:1 relationship for c values >2.9 Å, corresponding to $r_B \approx 0.6$ Å.

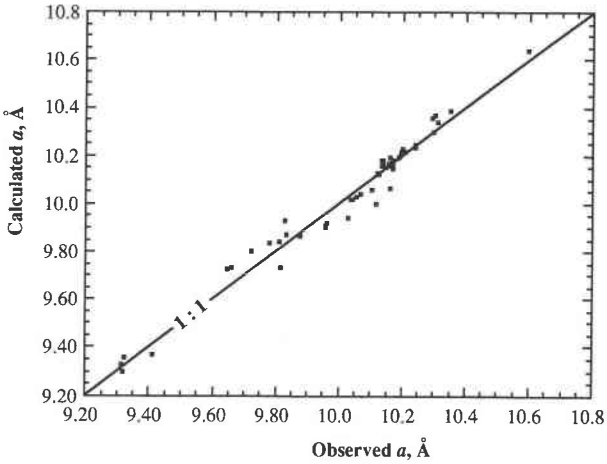

Fig. 3. Comparison of calculated and observed a values; calculated a values are based on Eq. 11.

= 2.975 Å), it can be seen that the a axis increases as the tunnel cation becomes larger, whereas the c axis is hardly affected. We therefore anticipate a dependence of a on δ_A, the amount by which r_A exceeds r_C, the radius of a perfectly fitting tunnel cation (see Eq. 1).

Equations 6 and 7, modified to include the anticipated dependencies of unit-cell parameters on octahedral cation valence, Z_B, and on the excess sizes of octahedral and tunnel cations, δ_B and δ_A, become

$$a = 5.130(r_O + r_B) + tZ_B + u\delta_A \quad (9)$$

$$c = \sqrt{2}(r_O + r_B) + vZ_B + w\delta_B. \quad (10)$$

We have determined optimal values for the coefficients t, u, v, and w by least-squares analysis using data for 48 of the 55 hollandite-type compounds listed in Table 1. Seven phases containing cations having two possible spin states were omitted from the analysis because the actual spin states of transition metal cations in hollandite are largely unknown, and effective high-spin and low-spin ionic radii are very different. The least-squares analysis yields the following equations for calculating the lengths of unit-cell edges:

$$a(\text{Å}) = 5.130(r_O + r_B) - 0.0291Z_B + 0.411\delta_A \quad (11)$$

$$c(\text{Å}) = \sqrt{2}(r_O + r_B) + 0.0366Z_B + 0.552\delta_B \quad (12)$$

where

$$\delta_A = \begin{cases} (r_O + r_A) - \sqrt{2}(r_O + r_B), & \text{if } r_O + r_A \geq \sqrt{2}(r_O + r_B) \\ 0, & \text{if } r_O + r_A < \sqrt{2}(r_O + r_B) \end{cases}$$

and

$$\delta_B = \begin{cases} r_B - 0.414r_O, & \text{if } r_B \geq 0.414r_O \\ 0, & \text{if } r_B < 0.414r_O. \end{cases}$$

Results and discussion

Unit-cell edges

The unit-cell edges of 55 hollandite-type phases calculated with Equations 11 and 12 are listed in Table 1. Most of the experimental data are from Donnay and Ondik (1973). The mean error for calculated a values is 0.036 Å, and that for calculated c values is 0.020 Å. The mean relative error is 0.36% for a and 0.67% for c. In Figures 3 and 4, the calculated a and c values are plotted vs. observed values. The points follow closely the 1:1 line, demonstrating that Equations 11 and 12 include appropriately the structural dependencies of unit-cell dimensions of hollandite-type compounds.

In some hollandite samples, distortions reduce the symmetry to monoclinic with $a \neq b$ and $\gamma > 90°$ (c axis unique). The deviations of unit-cell geometry from tetragonal are always small, with a and b differing only slightly and γ being no more than 2° greater than 90°. For this reason, we believe Equation 11 can be used to calculate satisfactorily the average of a and b for monoclinic phases, whereas Equation 12 is still applicable for calculating the length of c. Results for five monoclinic phases that confirm these assertions are listed at the bottom of Table 1.

Some hollandite-type phases contain OH^- in addition to O^{2-}. Because the two species have similar sizes (Shannon, 1976), Equations 11 and 12 are assumed to remain valid for such cases. The agreement between calculated and observed unit-cell edges for the OH^--containing phases listed in Table 1 appears as good as that for OH^--free compositions. Additionally, small amounts of H_2O incorporated in some hollandite-type phases appear to have negligible effects on unit-cell size.

Some of the transition metals occupying octahedral sites in hollandite can occur in either high- or low-spin state. Unit-cell edges calculated using high-spin radii agree bet-

TABLE 1. Comparison of observed and calculated *a* and *c* of hollandite-type compounds

No.	Composition	a_{obs}	a_{calc}	Diff.	c_{obs}	c_{calc}	Diff.
1	$K_2(Al_2Ti_6)O_{16}$	10.040	10.04	0.00	2.94	2.92	−0.02
2	$K_{1.78}(Al_{1.78}Ti_{6.22})O_{16}$	10.056	10.05	−0.01	2.94	2.92	−0.02
3	$K_{1.60}(Al_{1.60}Ti_{6.40})O_{16}$	10.067	10.06	−0.01	2.939	2.93	−0.01
4	$K_2(Ti_2^{3+}Ti_6^{4+})O_{16}$	10.170	10.21	0.04	2.958	3.00	0.04
5	$K_2(Cr_2Ti_6)O_{16}$	10.125	10.14	0.02	2.955	2.97	0.01
6	$K_2(Fe_2Ti_6)O_{16}$	10.148	10.18	0.03	2.969	2.99	0.02
7	$K_2(Ga_2Ti_6)O_{16}$	10.119	10.15	0.03	2.962	2.97	0.01
8	$K_2(MgTi_7)O_{16}$	10.157	10.20	0.04	2.974	3.00	0.03
9	$K_2(CoTi_7)O_{16}$	10.139	10.16	0.02	2.975	2.98	0.01
10	$K_2(NiTi_7)O_{16}$	10.140	10.19	0.05	2.965	2.99	0.03
11	$K_2(CuTi_7)O_{16}$	10.135	10.21	0.08	2.977	3.00	0.02
12	$K_2(ZnTi_7)O_{16}$	10.161	10.22	0.06	2.973	3.01	0.04
13	$Rb_2(Al_2Ti_6)O_{16}$	10.102	10.06	−0.04	2.941	2.92	−0.02
14	$Rb_2(Ti_2^{3+}Ti_6^{4+})O_{16}$	10.210	10.23	0.02	2.965	3.00	0.04
15	$Rb_2(Cr_2Ti_6)O_{16}$	10.168	10.16	−0.01	2.957	2.97	0.01
16	$Rb_2(Fe_2Ti_6)O_{16}$	10.189	10.20	0.01	2.976	2.99	0.01
17	$Rb_2(Ga_2Ti_6)O_{16}$	10.167	10.17	0.00	2.964	2.97	0.01
18	$Rb_2(MgTi_7)O_{16}$	10.195	10.22	0.03	2.975	3.00	0.03
19	$Rb_2(CoTi_7)O_{16}$	10.202	10.18	−0.02	2.978	2.98	0.00
20	$Rb_2(NiTi_7)O_{16}$	10.191	10.21	0.02	2.967	2.99	0.02
21	$Rb_2(CuTi_7)O_{16}$	10.196	10.22	0.02	2.980	3.00	0.02
22	$Rb_2(ZnTi_7)O_{16}$	10.203	10.23	0.03	2.976	3.01	0.03
23	$Ba_{0.75}Al_{1.5}Si_{2.5}O_8$	9.41	9.35	−0.06	2.72	2.71	−0.01
24	$Sr_{0.75}Al_{1.5}Si_{2.5}O_8$	9.32	9.33	0.01	2.72	2.71	−0.01
25	$RbAlGe_3O_8$	9.78	9.82	0.04	2.86	2.83	−0.03
26	$KAlGe_3O_8$	9.72	9.80	0.08	2.86	2.83	−0.03
27	$NaAlGe_3O_8$	9.648	9.77	0.12	2.856	2.83	−0.03
28	$TiO_2(H)$	10.161	10.12	−0.04	2.970	2.97	0.00
29	$KAlSi_3O_8$	9.315	9.30	−0.02	2.723	2.69	−0.03
30	$NaAlSi_3O_8$	9.30	9.24	−0.06	2.73	2.69	−0.04
31	$(Ba,K)(Mn,Mn,Fe,Al)_8(O,OH)_{16}$	9.96	9.92	−0.04	2.86	2.87	0.01
32	α-MnO_2	9.815	9.79	−0.03	2.847	2.85	0.00
33	$(Mg,Ca)(Ti,Cr,Si)_8O_{16}$	10.115	10.05	−0.07	2.94	2.93	−0.01
34	$K_2Li_{0.67}Ti_{7.33}O_8$	10.135	10.19	0.06	2.965	2.99	0.03
35	$Rb_2Al_5Sb_3O_{16}$	10.03	9.93	−0.10	2.94	2.87	−0.07
36	$K_2Al_5Sb_3O_{16}$	9.955	9.91	−0.05	2.94	2.87	−0.07
37	$K_2Ga_5Sb_3O_{16}$	10.165	10.19	0.03	3.01	2.99	−0.02
38	$K_2Cr_5Sb_3O_{16}$	10.17	10.17	0.00	3.015	2.98	−0.04
39	$K_2Ni_{3.33}Sb_{4.67}O_{16}$	10.30	10.34	0.04	3.07	3.06	−0.01
40	$K_2Fe_5Sb_3O_{16}$	10.24	10.26	0.02	3.06	3.03	−0.03
41	$K_2Zn_{3.33}Sb_{4.67}O_{16}$	10.35	10.43	0.08	3.10	3.11	0.01
42	$K_2Mg_{3.33}Sb_{4.67}O_{16}$	10.31	10.38	0.07	3.09	3.09	0.00
43	$K_2Cu_{3.33}Sb_{4.67}O_{16}$	10.295	10.40	0.11	3.095	3.10	0.01
44	$K_2Co_{3.33}Sb_{4.67}O_{16}$	10.305	10.41	0.11	3.10	3.10	0.00
45	$K_2In_2Sn_6O_{16}$	10.595	10.68	0.09	3.20	3.23	0.03
46	$K_2Mn_5Sb_3O_{16}$	10.24	10.28	0.04	3.11	3.04	−0.07
47	$(K_{0.90}Ba_{0.35})(Ti,Fe,Mg)_8O_{16}$	10.139	10.17	0.03	2.966	2.99	0.02
48	$(Ba_{0.98}Ca_{0.03}Zr_{0.02})(Al_{1.10}Ni_{0.48}Ti_{6.4})O_{16}$	10.039	10.06	0.02	2.943	2.93	−0.01
49	$TlAlGe_3O_8$	9.809	9.82	0.01	2.857	2.83	−0.03
50	$AgAlGe_3O_8$	9.662	9.77	0.11	2.860	2.83	−0.03
51*	$(Ca_{0.5}Mg_{0.5})Al_2Si_2O_8$	9.321	9.40	0.08	2.716	2.72	0.00
52*	$BaFeMn_7O_{16}$	9.955	9.94	−0.02	2.88	2.88	0.00
53*	$(Ba,Pb,K,Na)_{1.02}(Mn,Mn,Fe,Al,Si)_{7.86}$-$(O,OH)_{16}$	9.830	9.97	0.14	2.872	2.89	0.02
54*	$(Ba_{0.75}Pb_{0.16}Na_{0.10}K_{0.04})(Mn,Fe,Al)_8(O,OH)_{16}$	9.878	9.91	0.03	2.878	2.87	−0.01
55*	$(K_{0.94}Na_{0.25}Sr_{0.13}Ba_{0.10})(Mn,Fe,Al)(O,OH)_{16}$	9.831	9.90	0.07	2.871	2.87	0.00

* Monoclinic phase for which the calculated *a* is compared with the average of observed *a* and *b* (monoclinic first setting).

ter with experimental results than those calculated using low-spin radii. For example, the observed *a* of $Rb_2(Fe_2Ti_6)O_{16}$ of 10.189 Å compares more favorably with *a* of 10.19 Å calculated using the high-spin radius of Fe^{3+} (0.645 Å) than with *a* of 10.08 Å calculated with the low-spin radius (0.55 Å).

If the unit cell of an ideal hollandite with regular octahedra were to expand in response to substitution of a tunnel cation larger than the ideal size ($r_A > r_C$) without changing the thickness of the octahedral walls, the expected increase of *a* would be $4\delta_A\cos 30° = 3.46\delta_A$. The coefficient of δ_A in Equation 11 is, however, only 0.411, indicating that much of the tunnel cation radius increase is accommodated by thinning the octahedral walls rather than expanding *a*. This is consistent with observations at high pressure (Zhang et al., 1993) that show the wall becoming thinner as pressure increases, since increasing the size of the *A* cation should affect the octahedral framework the same way as subjecting the framework to compression (Hazen and Finger, 1982). Our assumption that the *c* axis is already so elongated from cation to cation repulsion that an excess-sized tunnel cation has little ef-

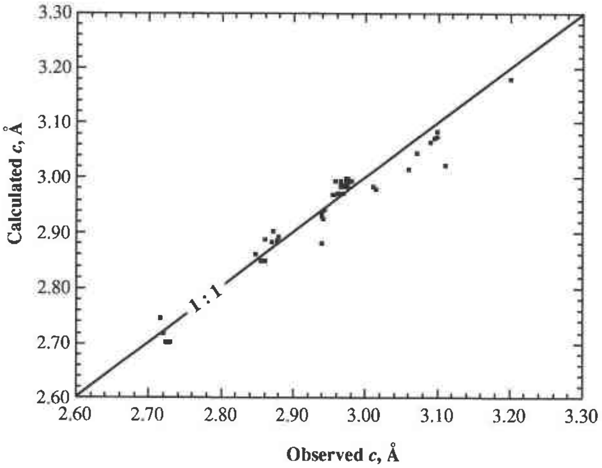

Fig. 4. Comparison of calculated and observed c values; calculated c values are based on Eq. 12.

fect is borne out by the excellent agreement of calculated with observed values (Fig. 3).

Finally, it might be possible to calculate the compressibilities of a and c using Equations 11 and 12, if the compressibility of the B-O bond is known either empirically or theoretically. If the variation of δ_A with pressure is negligible, then the compressibility along **a** will be the same as the compressibility of the B-O bond, because, with Equation 11,

$$\frac{1}{a}\frac{\mathrm{d}a}{\mathrm{d}p} = \frac{1}{a}\frac{\mathrm{d}}{\mathrm{d}p}[5.130(r_\mathrm{O} + r_B) - 0.0291 Z_B + 0.411\delta_A] \approx \frac{\mathrm{d}(r_\mathrm{O} + r_B)}{(r_\mathrm{O} + r_B)\mathrm{d}p}.$$

On the basis of data reported by Zhang et al. (1993), the compressibility of the (Si,Al)-O bond in hollandite-structured $KAlSi_3O_8$ is 1.85×10^{-3}/GPa in the range 0–4.47 GPa, and so the compressibility along **a** should also be 1.85×10^{-3}/GPa. This is in very good agreement with the experimental a-axis compressibility of $1.82(4) \times 10^{-3}$/GPa (Zhang et al., 1993).

From Equation 12, the c-axis compressibility is predicted to be

$$\frac{1}{c}\frac{\mathrm{d}c}{\mathrm{d}p} \approx \frac{\sqrt{2}}{c}\frac{\mathrm{d}(r_\mathrm{O} + r_B)}{\mathrm{d}p} = 1.74 \times 10^{-3}/\mathrm{GPa},$$

which is significantly larger than the experimental value of 1.04×10^{-3}/GPa. We believe this discrepancy is due to the strong cation to cation repulsions in the **c** direction. As the pressure increases, the coefficient v of Z_B in Equation 10 is expected to increase dramatically because of these B-B repulsions, causing the c-axis compressibility to be significantly smaller than the B-O bond compressibility. One might account for this effect by assuming that the decrease in c-axis compressibility due to cation to cation repulsions is proportional to octahedral cation charge.

Tetragonal vs. monoclinic symmetry

Two structural criteria have been proposed to predict hollandite symmetry. Sinclair et al. (1980) suggested that the symmetry change takes place at cell volumes between 290 and 300 Å³. Compounds having smaller unit cells should be tetragonal, and ones with larger unit cells monoclinic. Post et al. (1982) pointed out that this criterion has many exceptions and suggested instead that on a plot of average octahedral cation radius vs. average tunnel cation radius, a straight line with ratio $r_B/r_A = 0.48$ would separate tetragonal ($r_B/r_A < 0.48$) from monoclinic ($r_B/r_A > 0.48$) phases. This criterion also has many exceptions, and, in addition, it fails for phases without tunnel cations: α-MnO_2 and TiO_2(H) are both tetragonal despite their indeterminate r_B/r_A ratio.

Post and Burnham (1986) observed that tunnel cations in hollandite structures have anomalously large temperature factors that are, in part, manifestations of displacements from the $4/m$ special position. They suggested that the displacements increase as the tunnel cation becomes smaller and less constrained inside its coordination polyhedron. If the cation is small enough, the octahedral walls undergo twisting distortions to accommodate minimum energy cation positions closer to the nearer coordinating O atoms (Post et al., 1982). Such distortions cause the symmetry reduction, through which the attractive potential between the tunnel cation and its neighboring O atoms becomes asymmetric in directions perpendicular to **c**. Accordingly, if the size of the A cation is equal to or larger than the cavity formed by the octahedral framework, i.e., if $r_A \geq r_C$, the structure is likely to be tetragonal because the cation cannot move about in the cavity. So the upper limit for monoclinic symmetry would occur when the radius of the tunnel cation is equal to r_C, or from Equation 1,

$$r_A = \sqrt{2}(r_\mathrm{O} + r_B) - r_\mathrm{O}. \tag{13}$$

As r_A becomes smaller than r_C, the structure tends to become monoclinic, but it will tolerate some displacements of the tunnel cation before the onset of octahedral framework distortions causes the actual symmetry reduction. According to Post and Burnham (1986), refined tunnel cation temperature factors indicate root-mean-square displacements of 0.12–0.17 Å perpendicular to the tunnel direction at the $4/m$ special position. If we assume that an average value of 0.15 Å is the limit of tunnel cation displacement that tetragonal structures sustain without octahedral wall distortions, then the following equation defines a lower limit for tetragonal phases:

$$r_A = \sqrt{2}(r_\mathrm{O} + r_B) - r_\mathrm{O} - 0.15. \tag{14}$$

Thus we propose that if r_A is greater than that given by Equation 13, the symmetry should be tetragonal. If r_A is less than that given by Equation 14, the symmetry should be monoclinic. If r_A is intermediate between the two values, the symmetry can be either tetragonal or monoclinic, depending on other factors, such as the ordering of octahedral cations or the presence of irregular octahedral distortions. Because off-centering is moot in structures having no tunnel cations, such structures should always be tetragonal.

Figure 5, compiled using data from Post et al. (1982), indicates that Equations 13 and 14 correctly delineate (with one exception) the regions of tetragonal and monoclinic hollandite, with a region of overlap between them. These equations, which can be used to predict the symmetry of a hollandite-type phase, have a clear geometrical basis that includes a dependence on tunnel cation displacements from the special position.

$KAlSi_3O_8$ hollandite is tetragonal at room pressure. Zhang et al. (1993) observed that the KO_8 polyhedron compresses passively, i.e., the compressibility of the KO_8 polyhedron is dictated by changes in the $(Si,Al)O_6$ octahedral framework. It follows that the ratio of the tunnel cation (K^+) size to the octahedral cation size does not decrease with increasing pressure. Therefore the $KAlSi_3O_8$ hollandite will remain above the upper line in Figure 5 and is not expected to transform to lower symmetry at higher pressure.

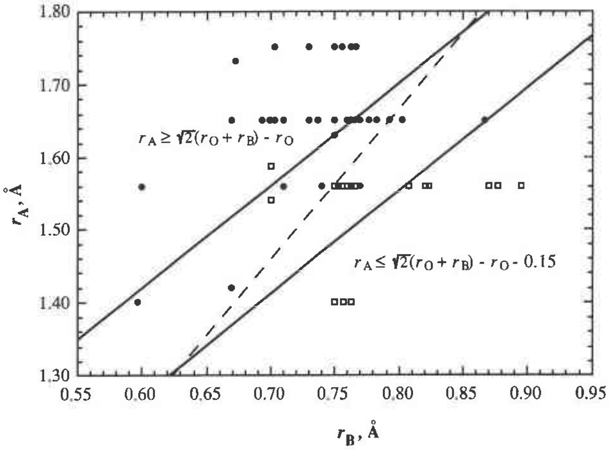

Fig. 5. Theoretical boundaries of symmetry compared with experimental data. Eqs. 13 (upper) and 14 (lower) divide the hollandite-type phases into three fields in the plot of average r_A vs. average r_B. The dashed line is the criterion $r_B/r_A = 0.48$ proposed by Post et al. (1982), from which all data are quoted.

Conclusions

The key component of the hollandite structure is the BO_6 octahedral framework. Assuming regular BO_6 octahedra, unit-cell edges can be estimated simply from the B-O bond distance. The real BO_6 octahedra, of course, are not regular, and the unit-cell size is not completely determined by the B-O bond distance. Strong B-B cation to cation repulsions elongate the c axis and shorten the a axis. If the tunnel cation is larger than the ideal size for its coordination polyhedron, its excess size expands the a axis. The increase in tunnel size brought on by an excess size of the A cation is largely offset by the thinning of the octahedral walls, and the result is just a slight increase in a as the excess size of the A cation increases. Finally, if the octahedral cation to anion radius ratio exceeds the classical critical value, the BO_6 octahedron undergoes further distortion, and more elongation along c results. Two simple equations embodying these factors can be used to estimate the lengths of a and c axes to about ± 0.04 and ± 0.02 Å, respectively.

The collapse of distorted octahedral walls around small tunnel cations causes hollandite-type phases to become monoclinic. When the tunnel cation is equal to or larger than the cavity formed by the surrounding O atoms, the cation cannot move around freely and is constrained to the center of the tunnel. The forces are centric, and the symmetry is tetragonal. When the tunnel cation is smaller than its cavity, it can be displaced from the $4/m$ special position, and that makes it easier for the octahedral walls to twist and collapse somewhat around the tunnel cation, causing the structure to adopt lower symmetry. The tetragonal structure tolerates tunnel cation displacements up to ~0.15 Å, but, if the cation is smaller than the cavity by more than about 0.15 Å, the octahedral walls twist, sometimes accompanied by movement of the small cations to off-centered positions, thereby lowering the symmetry to monoclinic. If the tunnel cation size is between these two limits, hollandite can be either tetragonal or monoclinic, depending on other factors such as, for example, octahedral distortions induced by the John-Teller effect or octahedral ordering.

Acknowledgments

This research was supported by National Science Foundation grant EAR-87-20666 to C.W.B. J.M.Z. wishes to thank Mark Van Baalen for useful discussions.

References cited

Beyeler, H.U. (1976) Cationic short-range order in the hollandite $K_{1.54}Mg_{0.77}Ti_{7.23}O_{16}$: Evidence for the importance of ion-ion interactions in superionic conductors. Physical Review Letters, 37, 1557–1560.

Burns, R.G., and Burns, V.M. (1977) The mineralogy and crystal chemistry of deep-sea manganese nodules, a polymetallic resource of the twenty-first century. Philosophical Transactions of the Royal Society of London, A286, 283–301.

Donnay, J.D.H., and Ondik, H.M. (1973) Crystal data: Determinative tables (3rd edition), vol. 2. U.S. Department of Commerce, National Bureau of Standards, and JCPDS.

Endo, T., Kume, S., Kinomura, N., and Koizumi, M. (1976) A new compound $K_2Cr_8O_{16}$ with hollandite type structure. Materials Research Bulletin, 11, 609–614.

Hazen, R.M., and Finger, L.W. (1982) Comparative crystal chemistry, 231 p. Wiley, New York.

Post, J.E., and Burnham, C.W. (1986) Modeling tunnel-cation displacements in hollandites using structure-energy calculations. American Mineralogist, 71, 1178–1185.

Post, J.E., Von Dreele, R.B., and Buseck, P.R. (1982) Symmetry and cation displacement in hollandite: Structure refinements of hollandite, cryptomelane and priderite. Acta Crystallographica, B38, 1056–1065.

Ringwood, A.E., Reid, A.F., and Wadsley, A.D. (1967) High-pressure $KAlSi_3O_8$, an aluminosilicate with sixfold coordination. Acta Crystallographica, 23, 1093–1095.

Ringwood, A.E., Kesson, S.E., Ware, N.G., Hibberson, W., and Major, A. (1979) Immobilisation of high level nuclear reactor wastes in SYNROC. Nature, 278, 219–223.

Shannon, R.D. (1976) Revised effective ionic radii and systematic studies of interatomic distances in halides and chalcogenides. Acta Crystallographica, A32, 751–767.
Shannon, R.D., and Prewitt, C.T. (1969) Effective ionic radii in oxides and fluorides. Acta Crystallographica, B25, 925–946.
Sinclair, W., McLaughlin, G.M., and Ringwood, A.E. (1980) The structure and chemistry of a barium titanate hollandite-type phase. Acta Crystallographica, B36, 2913–2918.
Zhang, J.M., Ko, J., Hazen, R.M., and Prewitt, C.T. (1993) High-pressure crystal chemistry of $KAlSi_3O_8$ hollandite. American Mineralogist, 78, 493–499.

Manuscript received December 22, 1992
Manuscript accepted September 21, 1993

Appendix 1. Atomic coordinates for ideal hollandite

Atomic coordinates for B, O1, and O2 atoms in an ideal hollandite $[A_{0-2}B_8(O,OH)_{16}]$ may be derived under the following assumptions: (1) $I4/m$ space-group symmetry; (2) B cations at the centers of regular O octahedra; (3) tunnel cations (A) at the centers of ideal square prismatic coordination polyhedra. Tunnel cations, A, occupy equipoint $2b$ ($4/m$) at 00½; octahedrally coordinated cations, B, and two crystallographically distinct O atoms, O1 and O2, occupy equipoints $8h$ (m) at $xy0$.

Referring to Figure 1, a c-axis projection of the ideal structure, observe that the horizontal projection of vector **AO1**, line segment AO1, is normal to the octahedral wall and has a length equal to ½ of the tunnel edge. From Equation 3

$$\mathrm{AO1} = \sqrt{6}(r_\mathrm{O} + r_B)/2. \qquad \text{(A1)}$$

Because $\angle \mathbf{a}\mathrm{AA'} = \pi/4$, the components of AO1 along x, $x_{\mathrm{O1}}\mathbf{a}$, and along y, $y_{\mathrm{O1}}\mathbf{b}$, are given by

$$x_{\mathrm{O1}}\mathbf{a} = \cos(\pi/4 + \angle\mathrm{A'AF})\cdot\mathrm{AO1}$$
$$y_{\mathrm{O1}}\mathbf{b} = \sin(\pi/4 + \angle\mathrm{A'AF})\cdot\mathrm{AO1} \qquad \text{(A2)}$$

where

$$\angle\mathrm{A'AF} = \sin^{-1}\left(\frac{\mathrm{A'F}}{\mathrm{A'A}}\right) = \sin^{-1}\left[\frac{\sqrt{6}/6\,(r_\mathrm{O} + r_B)}{3.627(r_\mathrm{O} + r_B)}\right]$$
$$= \sin^{-1}(0.1126) = 6.464°. \qquad \text{(A3)}$$

Values of A'F and A'A are from Equations 4 and 5, respectively. Note that $\angle$A'AF is constant for all ideal hollandite-type compounds. Substituting the ideal value of $\mathbf{a}$ [$= \mathbf{b} = 5.130(r_\mathrm{O} + r_B)$, Eq. 6], and the value of AO1 (Eq. A1) into Equation A2, we obtain $x_{\mathrm{O1}} = 0.1487$ and $y_{\mathrm{O1}} = 0.1868$.

Coordinates of O_2 are obtained from the components of vector **AO2**, where

$$\mathbf{AO2} = \mathbf{AO1} + \mathbf{O1O2}.$$

Let ϕ be the angle between **O1O2** and the direction of **a**. Then

$$x_{\mathrm{O2}}\mathbf{a} = x_{\mathrm{O1}}\mathbf{a} + \mathrm{O1O2}\cos\phi$$
$$y_{\mathrm{O2}}\mathbf{b} = y_{\mathrm{O1}}\mathbf{b} + \mathrm{O1O2}\sin\phi. \qquad \text{(A4)}$$

From Figure 1, we see that

$$\phi = (\pi/4 + \angle\mathrm{A'AF}) - \pi/2 + \angle\mathrm{JO1O2}. \qquad \text{(A5)}$$

The $\angle$JO1O2 is obtained from the geometry of the ideal octahedron, with B at the midpoint of O1O2, and JB equal to ½ the octahedral edge length:

$$\angle\mathrm{JO1O2} = \tan^{-1}(\mathrm{JB/O1B})$$
$$= \tan^{-1}[\sqrt{2}/2\,(r_\mathrm{O} + r_B)/(r_\mathrm{O} + r_B)] = 35.264°. \qquad \text{(A6)}$$

Substituting values from Equations A3 and A6 into Equation A5, we find $\phi = -3.273°$. Then substituting the ideal value of $\mathrm{O1O2} = 2(r_\mathrm{O} + r_B)$ and the value of ϕ into Equations A4, we obtain $x_{\mathrm{O2}} = 0.5380$ and $y_{\mathrm{O2}} = 0.1645$.

Noting that B is located at the midpoint of O1O2, we obtain

$$x_B = x_{\mathrm{O1}} + (x_{\mathrm{O2}} - x_{\mathrm{O1}})/2 = 0.3434$$
$$y_B = y_{\mathrm{O1}} + (y_{\mathrm{O2}} - y_{\mathrm{O1}})/2 = 0.1757.$$

From this analysis the atom coordinates of any ideal hollandite are

Atom	x	y	z
A	0	0	½
B	0.3434	0.1757	0
O1	0.1487	0.1868	0
O2	0.5380	0.1645	0.